

# Effect of mechanical milling of graphite powder on lithium intercalation properties

C. Natarajan<sup>\*</sup>, H. Fujimoto, A. Mabuchi, K. Tokumitsu, T. Kasuh

*Research & Development Department, Energy Technology Center, Osaka Gas Co. Ltd., 6-19-9, Torishima, Konohana-Ku, Osaka 554-0051, Japan*

Received 9 December 1999; received in revised form 2 June 2000; accepted 9 June 2000

## Abstract

Mechanically milled graphite powder for different durations was used as anode in lithium-ion battery. Reversible capacity and coulombic efficiency of the milled and pristine powders were measured. It was found that the controlled milling increases the reversible capacity and coulombic efficiency of the first cycle from 356 to 368 Ah kg<sup>-1</sup> and from 83 to 86%, respectively. The milled powder was analyzed for particle size distribution, bulk and surface structure by particle size analyzer, powder X-ray diffractometer, and Raman spectroscopy and electron microscope, respectively, to understand the effect of mechanical milling of graphite powder on its physical properties. The mild milling lead to aggregation of graphite particles, that had significant influences on the electrode performance. Graphite-tin dioxide composite electrode has also been prepared by the mechanical milling and the preliminary result indicates that the mechanical milling would be used to prepare the high capacity composite electrodes. © 2001 Elsevier Science B.V. All rights reserved.

*Keywords:* Mechanical milling; Graphite; Lithium-ion battery

## 1. Introduction

In the recent years, the research on the graphite anode for lithium ion battery has been focused towards improving the reversible capacity and reducing the irreversible capacity associated with the first charge cycle which limits the performance of the cells. The irreversible capacity in the first cycle has been controlled by modifying the surface and shape of the particle, and by manipulating the electrolyte [1]. The reversible capacity of the graphite anode has been improved to more than 400 Ah kg<sup>-1</sup> by oxidation [2,3], fluorination [4], mechanical milling [5] of graphite and also by producing composite electrodes with metal powders such as Si and Sn [6,7].

The mechanical milling process has been used to produce disordered carbon from graphite [5] and to produce the composite electrodes by milling the graphite with metal powder [6] for tens of hours. The milling of graphite powder for long duration yields highly disordered carbons with the particle size of few nanometer and crystallite size ( $L_c$ ) of 3–10 nm. Such milled carbon shows the reversible capacity of around 700 Ah kg<sup>-1</sup> and even the charge/discharge characteristics is very similar to that of the hard carbons

produced by synthetic route [8]. However, the irreversible capacity of the milled graphite drastically increases to more than ~350 Ah kg<sup>-1</sup>. Moreover, the surface area of the milled carbons is in the range of 100–500 m<sup>2</sup> g<sup>-1</sup>. But, the surface area of the carbon must be less than 10 m<sup>2</sup> g<sup>-1</sup> to ensure the safety of the lithium-ion battery. This indicates that the graphite milled for long duration with or without metal powder cannot be used in the commercial cells due to its large surface area and the irreversible capacity associated with it, in spite of the observed high reversible capacity. Nevertheless, we believe that the mechanical milling would be a good method to modify the shape and surface of the particle, and also to produce the composite electrodes, if the milling is done in a controlled manner for short duration. Recently, it has been disclosed in patents that increasing the rhombohedral phase fraction in the graphite, by mechanical grinding and ultrasonic treatment, could reduce the capacity loss in the first cycle [9,10].

We, therefore, decided to study the effect of the mechanical milling of the graphite powder for short duration on the physical and lithium intercalation properties. Based on the knowledge gained from this study, we made an attempt to produce the composite electrodes without damaging the graphite particles by controlling the milling of graphite powder with tin dioxide.

<sup>\*</sup> Corresponding author. Tel.: +81-6-6462-3436; fax: +81-6-6462-3436. E-mail address: rajan@tri.osakagas.co.jp (C. Natarajan).

## 2. Experimental

The graphite powder (commercial name SFG44, Timcal) was mechanically milled for different durations by using a ball mill (Retsch-planetary ball mill). The structural parameters of the milled powder were analyzed by using X-ray diffractometer (Rigaku-Rint-2500) with Cu  $K\alpha$  radiation. The lattice constant and crystallite size was determined from the full width half maximum (FWHM) of the  $d_{002}$  peak with Si as the internal standard. The particle size distribution was analyzed by using particle size analyzer (JEOL-Helos system). Brunauer–Emmet–Teller (BET) surface area was measured by using a Shimadzu surface area analyzer. The surface condition and morphology of the milled and pristine graphite were analyzed by using laser Raman spectroscopy (JRS-SYS1000) with a Ar-ion laser and a scanning electron microscope (JEOL), respectively.

Electrochemical measurements were made in a half-cell. The working electrodes were made by mixing graphite with 8% polyvinylidene difluoride (PVDF) in *N*-methyl pyrrolidine and the paste was coated on copper foil to 100 mm thickness by Doctor blade and pressed to 50 mm thickness. The electrode was cut in to a 1 cm  $\times$  1 cm and dried in vacuum at 200°C for 2 h. The electrode assembly was carried out in a dry glove box. The electrolyte used was 1 M LiClO<sub>4</sub> in ethylene carbonate and diethyl carbonate in 1:1 ratio. Lithium foils were used as counter and reference electrodes. The intercalation (charging) was carried out galvanostatically at 1 mA cm<sup>-2</sup> till the potential reaches 1 mV, then the charging mode was changed to potentiostatic mode. The total time for charging was 12 h. The deintercalation (discharging) was done by only galvanostatically at 1 mA cm<sup>-2</sup> till 2 V.

## 3. Results and discussion

### 3.1. Reversible and irreversible capacity

The reversible capacity ( $C_{\text{rev}}$ ) is defined as the lithium ion deintercalation capacity and the irreversible capacity ( $C_{\text{irr}}$ ) is defined as the difference between Li<sup>+</sup> intercalation and deintercalation capacity. Fig. 1 presents the reversible and irreversible capacity of the milled graphite as a function of milling time. The reversible and irreversible capacity of the as-received graphite powder are  $\sim 356$  and  $\sim 75$  Ah kg<sup>-1</sup>, respectively. When the powder is milled for 30–60 min, the reversible capacity increases to  $\sim 368$  Ah kg<sup>-1</sup> and the irreversible capacity decreases to  $\sim 60$  Ah kg<sup>-1</sup>. As a result, the current efficiency at the first cycle increases by  $\sim 3$ –86%. When the milling duration is extended beyond 5 h, the reversible capacity decreases drastically to  $\sim 290$  Ah kg<sup>-1</sup> and the irreversible capacity increases to  $\sim 106$  Ah kg<sup>-1</sup>. This brings down the coulombic efficiency at the first cycle to less than 73%. This indicates that the duration of the milling is very critical to the electrode performance.

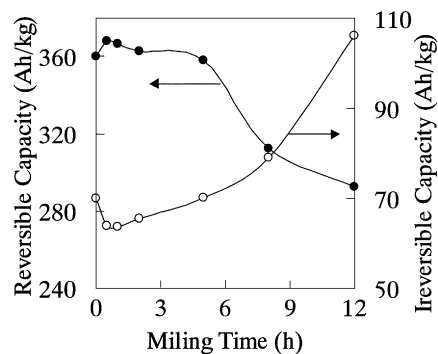


Fig. 1. Reversible and irreversible capacity of the milled graphite powder as a function of milling time.

In order to understand the influence of the mechanical milling on the charge/discharge behavior, the milled powders were analyzed for structural and morphological changes.

### 3.2. X-ray diffraction

Powder X-ray diffraction was used to analyze the bulk structure of the milled graphite powder. Inter planer distance ( $d$ ) and crystallite size in *c*-direction ( $L_c$ ) of the pristine powder is 3.354 Å and more than 1000 Å, respectively. The inter planer distance and the crystallite size do not change with milling time up to 12 h of milling, as the (0 0 2) peak position and FWHM do not change with milling time as shown in Fig. 2. However, the percentage of the rhombohedral phase changed with milling time and the same is presented in Fig. 3.

The pristine powder contains about 82% of hexagonal and 18% of rhombohedral phases. The relative fraction of the rhombohedral phase is derived by the ratio of the [1 0 1] X-ray diffraction line characteristics of rhombohedral phase to the sum of the areas of [1 0 1] lines of the phases present in

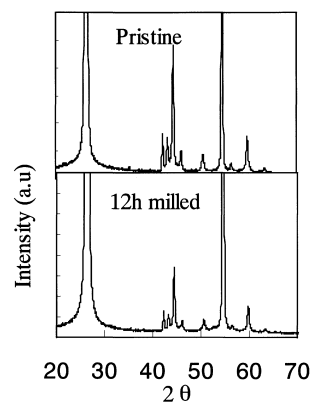


Fig. 2. Typical XRD pattern for the pristine and 12 h milled graphite powders.

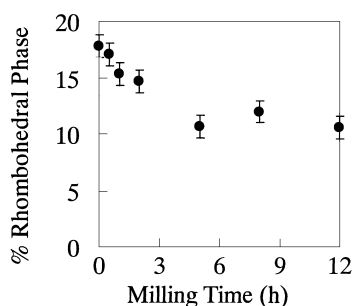


Fig. 3. Percentage of rhombohedral phase fraction as a function of milling time.

the material [9] and is given by Eq. (1)

$$\% \text{Rhombohedral fraction} = 100 \frac{\text{Rhombohedral}[101] \times 15/12}{\text{Rhombohedral}[101] \times 15/12 + \text{Hexagonal}[101]} \quad (1)$$

The rhombohedral phase fraction decreased with milling time and stabilized at  $\sim 10\%$  after 5 h of milling. From Figs. 1 and 3 one may conclude that  $C_{\text{irr}}$  decreases with decreasing rhombohedral phase fraction. But, Flandrois et al. [9] and Shi et al. [10] have disclosed in their patents that the  $C_{\text{irr}}$  decreases with increasing rhombohedral phase, which was modified by mechanical grinding and ultrasonic treatment. As the transformation energy of rhombohedral to hexagonal is very small, different types of milling might convert the rhombohedral (ABC) to hexagonal (AB) (and vice versa). This may be the reason for our observation of decrease and Flandrois et al. observation of increase in the rhombohedral phase fraction by mechanical milling. However, in both cases, it has been observed that the mild mechanical milling improves the electrode performance, irrespective of the percentage of rhombohedral phase in the graphite powder.

In order to clarify the effect of rhombohedral on the irreversible capacity, we measured the rhombohedral fraction and coulombic efficiency of SFG6, SFG10, SFG15 and SFG44. This set of material is manufactured from the same precursor by the same process [11]. This eliminates the ambiguity of phase transformation, by different types of millings. Fig. 4 presents the percentage of rhombohedral phase and current efficiency at the first cycle of the SFG series powder. One can see from the Fig. 4 that the current efficiency increases (decrease in the  $C_{\text{irr}}$ ) with decrease in the rhombohedral phase fraction. This trend is similar to the trend observed for the samples milled up to 5 h. Beyond 5 h the rhombohedral content (Fig. 3) is constant but the irreversible capacity kept increasing (Fig. 1). Therefore, this makes us to believe that there may be some parameters other than the rhombohedral phase, which influence the electrode performance of the milled powders.

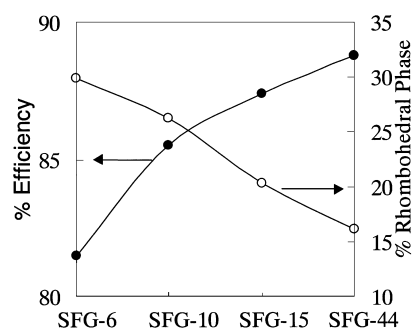


Fig. 4. Percentage of rhombohedral phase fraction and the current efficiency of SFG6, SFG10, SFG15 and SFG44 graphite powder.

### 3.3. Raman spectroscopy

The short duration of milling does not affect the crystalline size and inter planer distance, however, it might affect the surface condition of the particles. Therefore, the graphite powders were analyzed by Laser Raman spectroscopy to understand change in the surface structure with the milling. In general, carbon has two Raman bands, 1580 and 1360  $\text{cm}^{-1}$ , the latter being structure sensitive band assigned to a vibrational mode originating from the distorted hexagonal lattice of graphite near the crystal boundary [12]. The intensity ratio of 1360 and 1580  $\text{cm}^{-1}$  bands ( $R = I_{1360}/I_{1580}$ ) is proportional to the degree of structural disorder at the surface of the graphite. Fig. 5 presents the  $R$ -value derived from the Raman spectra for the pristine and milled graphite. The  $R$ -value of the pristine powder is 0.05, which indicates that the as received synthetic graphite itself contains some degree of structural defects on its surfaces. Upon increasing the milling time,  $R$ -value increases gradually indicating the increase of defects on the surface. But, the FWHM of 1580  $\text{cm}^{-1}$  peak is almost constant. This indicates that the crystallite size do not change with milling time up to 12 h. The Raman spectroscopic data reveals that the short duration milling does not alter the crystallite size but it increases the disorder on the surface. The increase in disorder cannot explain the improvement and decline of the electrode performance at the beginning and at long duration of the milling, respectively.

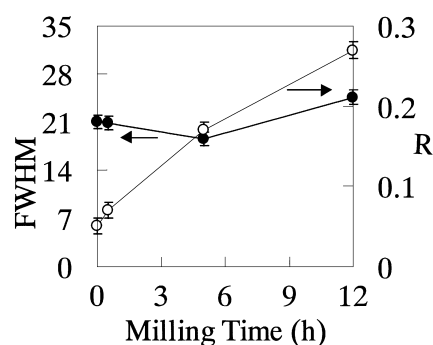


Fig. 5.  $R$ -value from Raman spectra and the full width half maximum of 1560  $\text{cm}^{-1}$  band as a function of milling time.

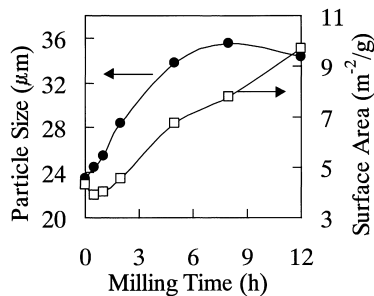


Fig. 6. Mean particle size and BET-surface area as a function of milling time.

### 3.4. Particle size and morphology analysis

Fig. 6 presents the mean particle size and the BET-surface area as a function of milling time. The mean particle size of the starting powders is 23.5 µm. The particle size increases with milling time and reaches a maximum of 35.5 µm at the eighth hour of milling and decreases beyond that time. The surface area of the graphite powder decreases at the beginning of the milling and increases gradually with milling time. One would normally expect that the particle size would decrease and the surface area would increase with milling time. On the contrary, we observed an increase in particle size and decrease in surface area at the beginning of the milling. This is due to aggregation of the smaller particles on the larger particles as evidenced by the particle size dis-

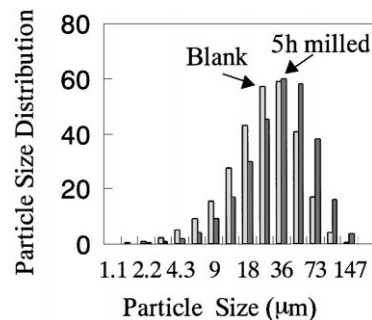


Fig. 7. Particle size distribution of pristine and milled graphite for 5 h.

tribution analysis and SEM as discussed later. We found similar aggregation phenomenon for short duration milling with other types of mills such as grinder and impact mills.

Fig. 7 presents the particle size distribution of the pristine and the milled powders for 8 h. As one can see, the milling process shifts the particle size distribution towards the larger size. This confirms that the short duration milling causes the aggregation of particles. Fig. 8 presents SEM micrographs of the pristine and milled graphite powders for 1–8 h. The shape of the pristine powder is flake with an average particle size of ~20 µm (Fig. 8A). When the powder was milled for 1 h, most of the flake particles become potato shaped particles with an average particle diameter of ~25 µm (Fig. 8B). The formation of potato shaped particle is noteworthy, as recently it has been reported that spherical

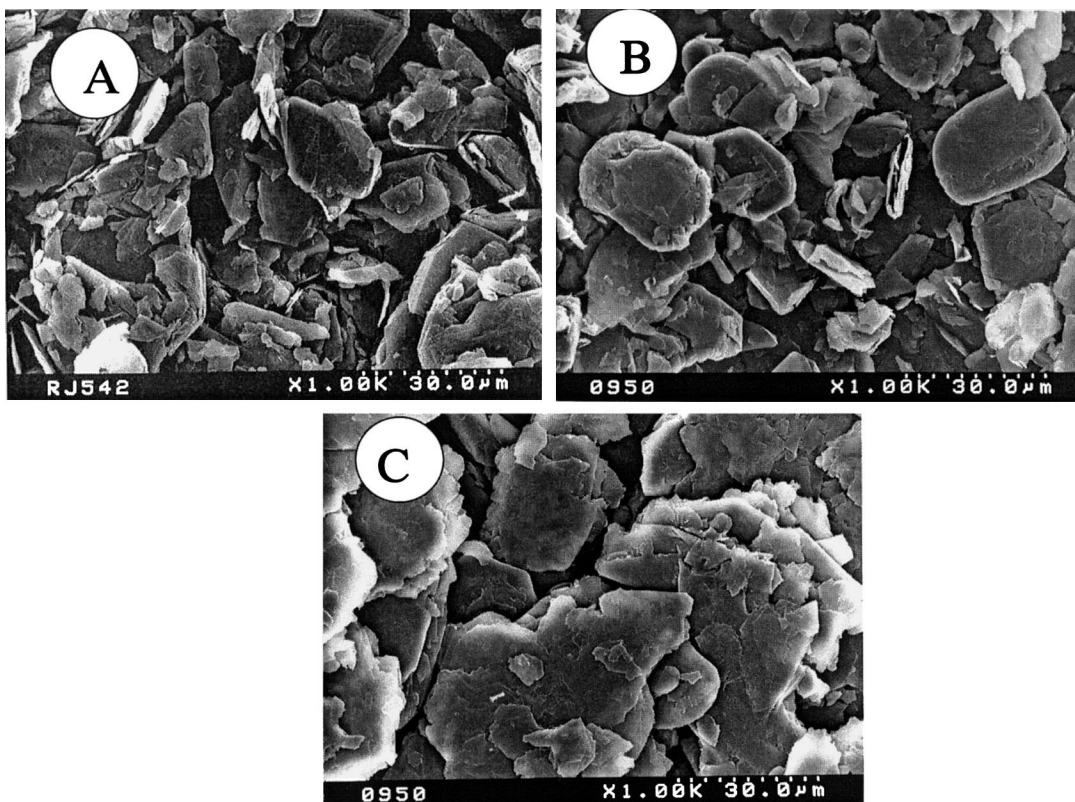


Fig. 8. SEM micrograph of (A) pristine; (B) 1 h; (C) 8 h milled graphite powders.

particle improves the electrode performance [13]. Therefore, the decrease in the  $C_{\text{irr}}$  for 30–60 min milled powder may be attributed to the potato shaped particles. When it was milled for more than 5 h, the potato shape of the particle is destroyed and aggregation increases, which results in the mean particle size of  $\sim 35 \mu\text{m}$  (Fig. 8C). Moreover, one can note from the SEM that the aggregation occurs on the basal plane surface than the edge surface.

The decrease in the surface area of the powders milled up to 60 min is also due to the aggregation. The process of aggregation has created nano cavities in between the particles, which become inaccessible to nitrogen molecules, resulting in the lower BET surface area. When the milling duration is extended beyond 1 h, the aggregation still continues but the surface area also increases. This may be due to two reasons; (1) the micro cavities generated at the beginning of the milling are made accessible to nitrogen molecules by the extended milling and (2) due to the shear interaction of the ball milling, splitting of the particle occurs along the basal plane. Either of the above or both reasons might be responsible for the increase in the surface area, while the mean particle size increases. The distribution of particle size analysis and surface analysis reveal that the short duration milling leads to potato shaped particles with little aggregation and extended milling leads to splitting of the aggregated particles with irregular shapes.

### 3.5. Mechanism

The change in the electrode performance with milling may be explained by a simplified illustration in Fig. 9. In general, there are many reasons for the irreversible capacity at the first cycle; such as SEI film formation, solvent decomposition and exfoliation of the graphite. The exfoliation of the graphite by the intercalation of solvated lithium ion occurs at the end of the interlayer spacing and at the defective sites at the basal plane, where the binding Vander-walls force between graphene sheets is less than the bulk

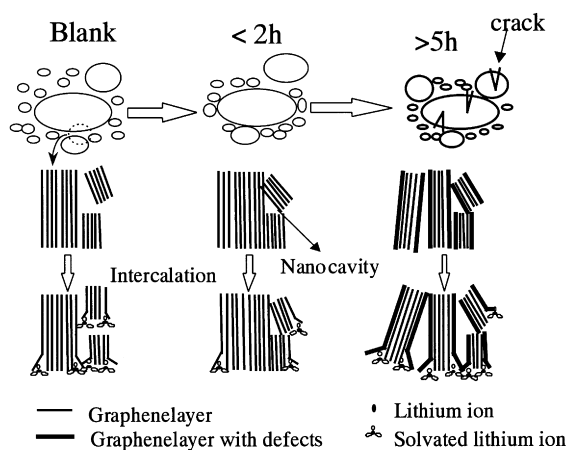


Fig. 9. Schematic diagram showing the intercalation of  $\text{Li}^+$  and exfoliation of the milled graphite powders.

sheets. Since, the particles of the graphite powders as received are loosely bounded to each other, the end of the basal plane sites are susceptible for exfoliation and leads to irreversible capacity [11].

When the powders are milled for short duration (less than 2 h), the potato shaped particles are formed and aggregation also takes place. The formation of potato shaped particle and the aggregation phenomena are responsible for the reduction in the surface area. Though it is generally accepted that the irreversible capacity is proportional to the surface area, particularly to the basal plan surface area [11]. The aggregation reduces the basal plane surface area as evidenced from the surface area measurement and SEM micrograph, consequently, reducing the number of sites to be exfoliated. As a result, the reversible capacity increases and irreversible capacity decreases for the powder milled for less than 2 h. When the powders are milled for long time (more than 5 h), the particles are likely to crack along the basal plane due to the shear interaction nature of the milling. This increases the surface area of the basal plane or in other words increases the number of sites prone to exfoliation, which increases the irreversible capacity and as well lead to the loss of reversible capacity. It reveals that the graphite powder cannot be milled for more than 5 h during the process of electrode fabrication. However, the time duration of the milling varies and depends on the method of milling and nature of the graphite powder.

### 3.6. Composite electrode

We made an attempt to produce graphite–tin dioxide composite electrode by mechanical milling. Three composite electrodes were prepared at three milling conditions; (A) graphite with 10% of  $\text{SnO}_2$  was milled for 1 h, (B) graphite with 10% of  $\text{SnO}_2$  was milled for 20 h and (C) 10% of pre-milled  $\text{SnO}_2$  powders was milled with graphite for 1 h. Typical charge/discharge curves of these composite electrodes are shown in Fig. 10. The electrode ‘A’ shows  $\sim 357$  and  $\sim 97 \text{ Ah kg}^{-1}$  as reversible and irreversible capacity, respectively. The reversible capacity of electrode ‘A’ is less than  $372 \text{ Ah kg}^{-1}$ , though it contains 10% of high capacity  $\text{SnO}_2$ . This is because the 1 h milling is not sufficient to break

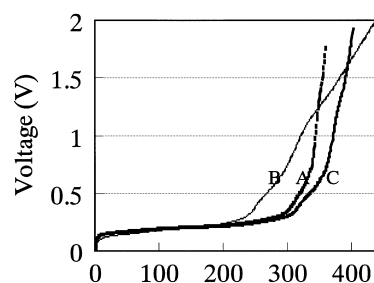


Fig. 10. Charging curves of the composite electrodes of SFG44 + 10% of  $\text{SnO}_2$  with different milling duration. A — Graphite + 10% of  $\text{SnO}_2$  milled for 1 h, B — Graphite + 10% of  $\text{SnO}_2$  milled for 20 h and C — Graphite + 10% of pre-milled  $\text{SnO}_2$  milled for 1 h.

25  $\mu\text{m}$   $\text{SnO}_2$  into sub-micron size particle. The electrode 'B', produced by 20 h milling, shows  $\sim 435$  and  $\sim 603$   $\text{Ah kg}^{-1}$  as reversible and irreversible capacity, respectively. In this case, the milling time is sufficient to mill the  $\text{SnO}_2$  into sub-micron size particle, which leads to the utilization of the maximum portion of  $\text{SnO}_2$  resulting in high capacity. At the same time, the 20 h of milling transforms the graphite into highly disordered carbon, which increase the irreversible capacity to very high level. The electrode 'C' shows  $\sim 401$  and  $\sim 99$   $\text{Ah kg}^{-1}$  as reversible and irreversible capacity, respectively. In this case the  $\text{SnO}_2$  is pre-milled to sub-micron size and then mixed with graphite powders and further milled for only 1 h. Therefore, this electrode gives high reversible and low irreversible capacity. In fact, if one compares the reversible capacity at 1 V cut-off potential, the electrode 'C' shows highest capacity. These preliminary results suggest that the mechanical milling would be used to produce high capacity composite electrode, if it is milled in a controlled manner.

#### 4. Conclusion

The short duration milling of graphite powders improves anode performance in the lithium-ion battery. This improvement in capacity and current efficiency is attributed to the aggregation and potato shaped particles formation. The aggregation inhibits the graphite exfoliation by co-intercalation of solvent molecules resulting in the improvement of the electrode performance. However, extended milling destroys surface and increases the basal plane surface area, which reduces the reversible capacity and increases the irreversible capacity. Therefore, it should be noted that the graphite powders could not be milled for more than 5 h during the fabrication of either pure graphite or compo-

site electrode with metal powders. The composite electrode with 10% of tin dioxide produced by short duration milling shows 401  $\text{Ah kg}^{-1}$  and 80% as current efficiency at the first cycle.

#### Acknowledgements

The New Energy and Industrial Technology Development Organization (NEDO) supported this work and one of the authors (C.N).

#### References

- [1] Y. Ein-Eli, *Electrochem. Solid-State Lett.* 2 (1999) 212.
- [2] C. Menachem, E. Peled, L. Burstein, Y. Rosenberg, *J. Power Sources* 68 (1997) 277.
- [3] Y. Ein-Eli, V.R. Koch, *J. Electrochem. Soc.* 144 (1997) 2968.
- [4] T. Nakashima, M. Koh, M. Shimada, R. Shing, T. Shirasaki, A. Tressaud, in: *International Symposium on Carbon Science and Technology for New Carbons, Japan, 1998*, p. 396.
- [5] F. Disma, L. Aymard, L. Dupont, J.-M. Tarascon, *J. Electrochem. Soc.* 143 (1996) 3959.
- [6] C.S. Wang, G.T. Wu, X.B. Zhang, Z.F. Qi, W.Z. Li, *J. Electrochem. Soc.* 145 (1998) 2751.
- [7] J.O. Besenhard, J. Jang, M. Winter, *J. Power Sources* 68 (1997) 87.
- [8] K. Tokumitsu, A. Mabuchi, H. Fujimoto, T. Kasuh, *J. Electrochem. Soc.* 143 (1996) 2235.
- [9] S. Flandrois, A. Fevrier, P. Biensanand, B. Simon, United States Patent No. 5,554,462 (1996).
- [10] H. Shi, J. Barker, R. Koksang, United States Patent No. 5,700,298 (1997).
- [11] M. Winter, P. Novak, A. Monnier, *J. Electrochem. Soc.* 145 (1998) 428.
- [12] M. Nakamizo, H. Honda, M. Inagaki, *Carbon* 16 (1978) 281.
- [13] Y. Nishi, in: *Proceedings of the POWER'98, Santa Clara, CA, USA, 1998*.